Thermoplasticized Bread Waste and Poly(butylene adipate-co-terephthalate) Blends: A Sustainable Alternative to Starch in Eco-Friendly Packaging

Samar Bouzidi, Jean-Marc Lévèque, Albert Magnin, Sonia Molina-Boisseau, Jean-Luc Putaux, Sami Boufi

ACS Sustainable Chemistry & Engineering

pubs.acs.org/journal/ascecg

Research Article

Thermoplasticized Bread Waste and Poly(butylene adipate-*co*-terephthalate) Blends: A Sustainable Alternative to Starch in Eco-Friendly Packaging

Samar Bouzidi, Jean-Marc Lévèque, Albert Magnin, Sonia Molina-Boisseau, Jean-Luc Putaux, and Sami Boufi*

Cite This: *ACS Sustainable Chem. Eng.* 2024, 12, 15268−15281

Read Online

ACCESS | Metrics & More | Article Recommendations

ABSTRACT: Bread and derived products are among the most wasted food in the developed world, with more than 30% of unsold and subsequently thrown away daily goods, causing significant environmental harm (disposal, transportation, etc.) and substantial economic losses. The main constituent of these products is starch-rich flour, which is mixed with water and minor components such as salt and lipids before baking. Valorizing this bread waste (BW) by taking advantage of its high polysaccharide content would be highly desirable. In the present work, BW was used as an inexpensive source of starchy material and a replacement of native starch that does not compete with food crops. Biodegradable plastics were produced by plasticizing BW with glycerol in a ratio from 85/15 to 80/20 (w/w) to produce thermoplasticized BW (TPB), which was then mixed with poly(butylene adipate-*co*-terephthalate) (PBAT) in a weight ratio varying from 70/30 to 50/50 in the presence of a compatibilizing agent using a melt-processing route to produce pellets and thin films. The morphology of the resulting materials, their mechanical and thermal properties, and their moisture sorption as a function of the TPB content and compatibilization were investigated. Satisfactory mechanical and moisture resistance was achieved with a TPB content of up to 40 wt % in the presence of a small amount of added PBAT-grafted maleic anhydride as a compatibilizing agent. A pilot extrusion-blowing test was run with a 60/40 (w/w) PBAT/TPB blend, resulting in uniform ∼30 μm-thick films free of defects. This proof of concept demonstrates the possible replacement of edible starch with BW to reduce food waste for the production of biodegradable plastic packaging, with potential applications as consumer bags, packaging, and agricultural mulch films, among others.

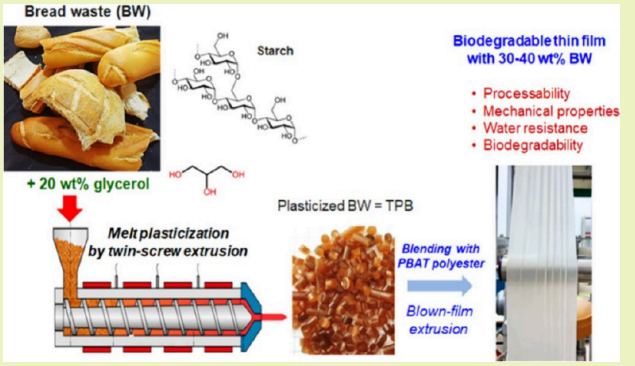

KEYWORDS: *bread waste, poly(butylene adipate-co-terephthalate), extrusion, biodegradability, blends, films*

1. INTRODUCTION

Almost all plastic materials developed by humans originate from petrosourced products. With less than 20% of plastic waste recycled, and more than 25% incinerated[1] most of the remaining plastic waste (around 60%) is landfilled, causing serious environmental pollution problems, with the most severe being the widespread micro- and nanoscale plastic pollution.[2] These tiny particles are generated from the slow but persistent breakdown of plastic waste into smaller, hardly biodegradable plastic fragments, under the concomitant action of natural physical, chemical, and biological processes. Their unstoppable mobility stemming from their microscopic size and ability to travel through multiple transportation pathways, has resulted in the worldwide contamination of soils, oceans, rivers, and water.[3] These microplastics have become an emerging global concern in recent years due to the potential health risks they pose to ecosystems and humankind through the food chain. This threat is even aggravated by the risk of leaching and lixiviation of chemical additives that are incorporated into plastic polymers to facilitate their processing and increase their physicochemical properties like their resistance to degradation. All of these adverse environmental impacts of fossil plastics along with the increasing government regulations toward the ban of single-use plastic have increased the wariness on this class of material and encouraged the consumer to choose environmentally friendly biodegradable

Received: August 17, 2024
Revised: September 22, 2024
Accepted: September 23, 2024
Published: October 1, 2024

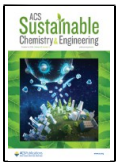

plastics that are more or less easily decomposed by the action of living organisms such as microbes, enzymes, bacteria, etc.

Nowadays, starch-based biodegradable plastics (SBPs) are an important class of biodegradable plastics representing more than 15% of the total bioplastic production capacity.[4] They are widely used in various applications featuring flexible and rigid packaging such as thermoformed trays and containers.[5,6] They are also commonly used in agriculture and horticulture for applications such as mulching or covering film to improve microclimate for crop growth, conserve soil moisture, and promote seedling growth with less need for chemical agents.[7,8] The reasonable price and wide availability of starch coupled with its environment-friendly character and its ready biodegradability are the main drivers for a steady growth of the industrial production of SBPs. The biodegradability of starch-blended polymers may allow safe disposal in natural environments, where microorganisms can break them down into nontoxic byproducts that are themselves biodegradable. This makes them ideal candidates to substitute single-use and nonbiodegradable oil-based plastics in packaging materials and disposable cutlery and appears as a promising solution for reducing plastic waste while promoting a sustainable future.

SBPs are made from starch mixed with thermoplastic polyesters to create biodegradable and compostable products that combine the respective advantages of starch with those of polyesters. In addition, SBPs can be processed using conventional techniques such as extrusion, injection molding, and blown extrusion for thin films, without the need for any special equipment. However, one of the major challenges faced by SBPs as raw materials is the competition with food resources since edible starches from corn, wheat, or potato, currently used for the production of SBPs, are also essential food crops worldwide. This allocation of starch for nonfood purposes would inevitably drive up food prices and negatively impact the supply of raw materials, leading to price fluctuations in the food market. This fact does not align with the principle of sustainability, even though the current use of starch in the production of bioplastics remains relatively low as compared with its food utilization, which is the argument put forward to justify the use of starch as feedstocks in Bioplastic production.

To minimize competition with food crops, it is therefore crucial to focus on sustainable sourcing practices for the starch used in bioplastics. In this context, the use of nonfood feedstocks such as food waste, underutilized crop residues, and nonedible parts of plants constitutes an attractive and necessary option that would positively promote the transition to a circular and biobased economy for biodegradable plastics.

Bread and bakery products are among the most consumed food items in the world but also some of the most wasted foods. Every year, millions of tons of bread are wasted worldwide because of their rapid spoilage, and their aspect and property change upon aging. In Europe, more than 30 vol % of bread is wasted in households and supermarkets, largely due to unsold surplus products. For instance, In France, every year, around 500,000 tons of bread are thrown away, representing more than €1.9 million in commercial losses, without considering the additional costs of storage, transportation, disposal, and destruction. Bread waste (BW) represents a substantial untapped starch-rich resource, accounting for more than 80% of bread (based on dry weight), and the rest is composed of 13−18% proteins (from gluten) and 2−4% lipids. The high polysaccharide content of BW makes it a promising candidate for recycling in fermentation processes, as it serves as an excellent feedstock for the growth of microorganisms such as bacteria, fungi, and yeasts. In that sense, several papers have reported on the use of BW as a potential bioresource for the production of fermentable sugars[9] and bioethanol using crude hydrolytic enzymes,[10] and succinic acid.[11] The potential use of BW as a functional ingredient in the production of extruded and baked maintenance diet food formulations for pets to enhance sustainability and reduce food waste in the industry was also recently reported.[12] One may also consider the possibility of using BW as an economical feedstock to replace wholly or partially edible starch to develop bioplastics. However, this option has not been so far explored, more specifically for starch-based biodegradable plastics, hence the motivation of the present work. Presently, food-grade starch originating from crops has been replaced by BW to produce SPBs after a plasticization step of ground BW by melt-extrusion in the presence of glycerol to produce thermoplasticized bread waste (TPB) in the form of pellets, that were subsequently blended with poly(butylene adipate-*co*-terephthalate) (PBAT). To our knowledge, the replacement of starch with BW in SPB has not been reported so far and is worth investigating to contribute to a more sustainable route for the production of biodegradable plastics as part of a circular economy. Therefore, in this work, we investigated how fully replacing starch with BW would impact the properties of blends based on PBAT and TPB, and compared the results with those obtained using food-grade starch.

2. MATERIALS AND METHODS

Materials. The bread waste (BW) was collected from a local bakery, and the same composition was used for all the work after milling. It corresponds to conventional bread made solely from wheat flour, water, salt, and yeast. Poly(butylene adipate-*co*-terephthalate) (Ecoflex F blend C1200) was purchased from BASF Chemical Company, and glycerol (G), maleic anhydride (MA), and benzoyl peroxide (BP) were purchased from Sigma−Aldrich.

BW Milling. The BW was ground into uniform granules with an average size between 0.5 and 1.0 mm using a laboratory hammer grinding mill (Polymix PX-MFC 90 D), composed of a rotor with three hardened strike hammers and a grooved stator. During the grinding process, the sample was spun around the grinding chamber and struck until the desired particle size was achieved. The ground sample passed through a 1 mm sieve into the collection container.

Maleated PBAT (PBAT-*g*-MA). PBAT-*g*-MA was prepared by grafting PBAT with MA in the TSE using BP as a radical source, following the method described in our previous work.[13] The as-prepared PBAT-*g*-MA showed a degree of maleation of approximately 1.5 wt %.

Themoplasticized Bread Waste (TPB) Processing and PBAT/TPB Blending. TPB was prepared by melt-extrusion of BW with glycerol as follows: BW was first milled into a coarse powder using a kitchen-milling machine, and then mixed with glycerol at the appropriate ratio (15−20 wt %) with the addition of 10 wt % water, and left for 3 h at room temperature to ensure absorption of G and water. Where applicable, aqueous MA was directly added to the mixture. Next, the BW/G mixture was extruded using a twin-screw extruder (TSE) (Letsritz 18 MAXX) with a screw diameter of 18.5 mm and a screw length of 32D. The extruder was equipped with a conical volumetric feeder. The screw operated at a speed of 100 rpm, and the temperature profile was set to 125/125/130/130/130 °C across the five heating zones. The TPB was extruded in the form of filaments of 3 mm in diameter, pelletized in granules, dried at 70 °C for at least 6 h to ensure the complete removal of water, and stored in a closed container away from humidity. It is worth mentioning that after extrusion, homogeneous elastic materials were obtained. The plasticized BW will be referred to as TPB-X-Y hereafter, where X and Y correspond to the weight contents of G and MA, respectively.

https://doi.org/10.1021/acssuschemeng.4c06823
ACS Sustainable Chem. Eng. 2024, 12, 15268−15281

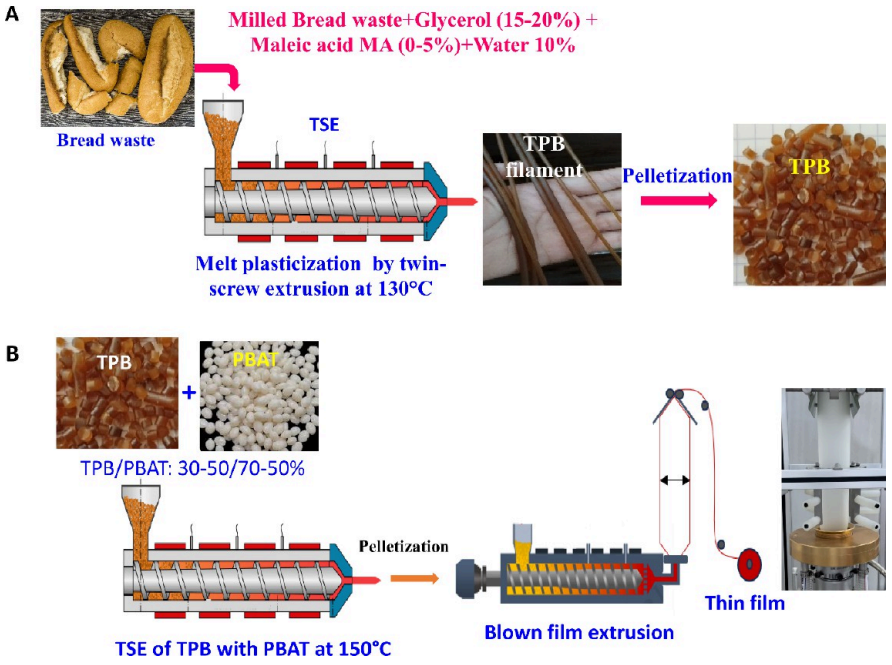

Figure 1. Illustration of the different processing steps involved in (A) the preparation of TPB and (B) blending of TPB with PBAT and the subsequent blown-film extrusion to produce thin films.

The blending of TPB with PBAT was compounded by mixing the appropriate PBAT and TPB pellets and feeding in the TSE (the same as for TPB processing) with a temperature profile set at 130/140/150/145/140 °C, respectively in the five-heating zones. The blend was either delivered as 3 cm-wide and 0.2 mm-thick thin films using a flat die or in the form of filament when pelletizing is needed. The blends will be referred to as PBAT/TPB X-Y-Z, where X, Y, and Z are the weight content of PBAT, TPB, and PBAT-*g*-MA compatibilizer. Figure 1 schematizes the different sequences of processing of the TPB alone and blends of TPB and PBAT to produce thin films by blown extrusion.

Preparation of PBAT/TPB Blown Films. The blown film test was conducted as follows: Pellets of the PBAT/TPB 60/40 blend were dried at 70 °C for 4 h, then fed into the hopper of a single-screw film-blowing pilot extrusion machine (SCM20) with a screw diameter of 20 mm and a length-to-diameter ratio of 28:1, manufactured by Lianjiang Machinery in Zhangjiagang (China). The extruder temperature was set to 130/135/138/140/145 °C across the five zones, with the screw running at 500 rpm. The die temperature was maintained at 145 °C. As the material exited the die, air was used to blow a bubble, which was then pulled away by take-up rollers operating at a constant speed. The blown bubble was flattened by nip rollers and collected by take-up rollers.

The blow-up ratio (BUR) was calculated by dividing the diameter of the bubble (D_b) by the diameter of the die (D_d):

$$\mathrm{BUR} = \frac{D_b}{D_d} \tag{1}$$

The bubble diameter can be calculated as $D_b = 2 \times (\text{lay flat width}/\pi)$. The draw-down ratio (DDR) corresponds to the decrease in the final thickness of the melt following the blowing process and was determined as

$$\mathrm{DDR} = \frac{\text{die gap}}{\text{film thickness}} \times \frac{1}{\mathrm{BUR}} \tag{2}$$

The blowing and processing parameters are presented in Table 1.

Tensile Tests. Tensile tests were carried out using an Instron tensile testing machine equipped with a 2.5 kN load cell, operating at a strain rate of 50 mm min^{-1}. The tests were conducted following the ISO 527-3 standard procedure. Before testing, the samples were conditioned at 25 °C and 50% relative humidity (RH) for 72 h. Ten specimens were tested for each composition.

Table 1. Blowing and Processing Parameters

Lay flat-width	120 mm
Bubble diameter (D_b)	39 mm
Die diameter (D_d)	45 mm
Die gap	0.8 mm
Film thickness	0.04 mm
Blow-up ratio (BUR)	1.69
Draw-down ratio (DDR)	11.8

Rheology. Rheological properties were analyzed using a controlled rate dynamic rheometer (Pro+ Kinexus from Malvern) with a plate geometry and a 1 mm gap. The storage modulus (G'), loss modulus (G''), and complex viscosity (η^*) of the blend systems were measured as a function of angular frequency, ranging from 0.01 to 10 Hz at 150 °C. Before each measurement, an amplitude sweep was conducted within the deformation range of 0.1−100% at angular frequencies of 0.01 and 10 Hz to determine the linear viscoelastic region. The deformation during the frequency sweeps was then set to remain within this linear viscoelastic region.

Morphological Characterization. Cross sections of the extruded samples were obtained after fracturing the films in liquid nitrogen. To improve the contrast and better discern the constituting phases, the cryofractured sections were soaked in a 1 N HCl solution for 2 h at 50 °C to remove TPB. After rinsing in water and drying, the film fragments were fixed onto metallic stubs with double-sided carbon tape, and coated with Au/Pd in a Safematic CCU-010-HV sputter coater. Secondary electron images were recorded with a Thermo Scientific Quanta FEG 250 microscope operating at 2.5 kV.

Fourier Transform Infrared (FTIR) Spectroscopy. FTIR-ATR spectra were recorded with a PerkinElmer Spectrum II spectrometer equipped with a diamond crystal plate ATR MIR single-reflection accessory, with a resolution of 4 cm^{-1}, over the range of 500 to 4000 cm^{-1}.

X-ray Diffraction (XRD). BW was ground into a fine powder that was poured into a 1 mm (outer diameter) glass capillary that was subsequently flame-sealed and taped onto a metallic collimator, while strips of blend film were directly fixed onto the collimator. All

https://doi.org/10.1021/acssuschemeng.4c06823
ACS Sustainable Chem. Eng. 2024, 12, 15268−15281

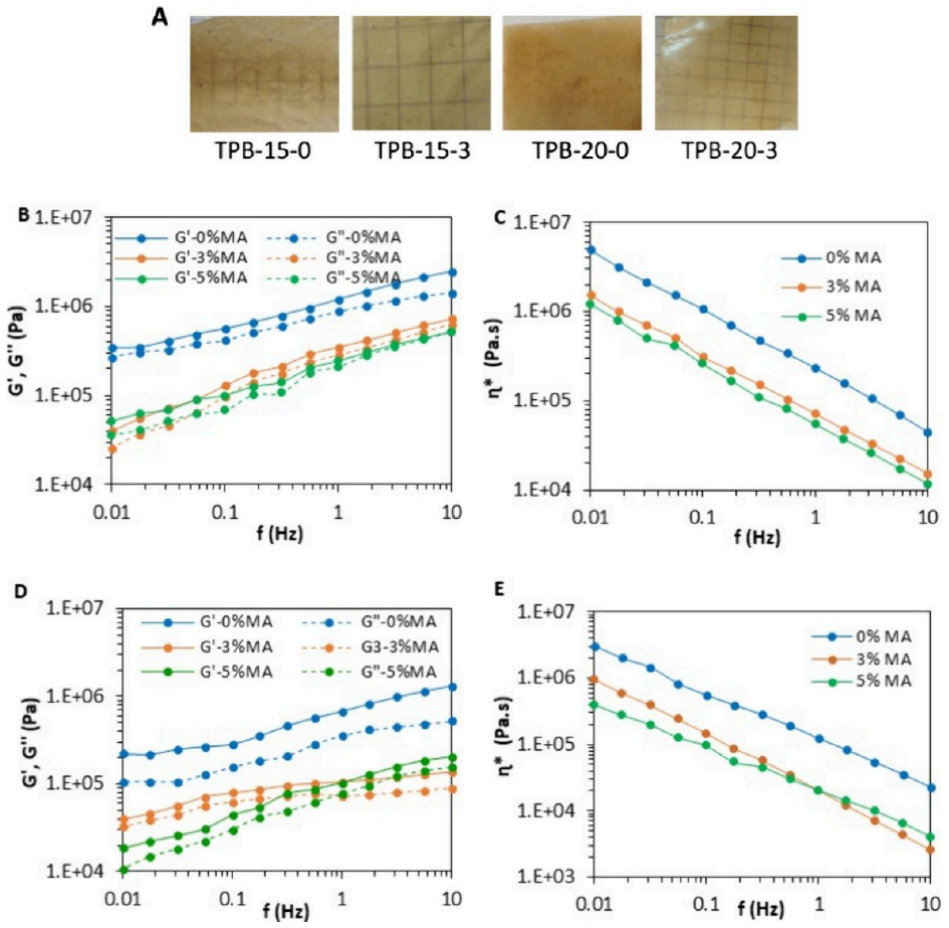

Figure 2. (A) Visual aspect of the TPB films. (B, D) Storage modulus (G') and loss modulus (G'') for TPB in the presence of different amounts of MA at (B) TPB-15-MA, (D) TPB-20-MA. (C, E) Corresponding complex viscosity (η^*) vs frequency for (C) TPB-15-MA and (E) TPB-20-MA at 150 °C.

specimens were X-rayed in vacuum using a Philips PW3830 (30 kV, 20 mA, Ni-filtered Cu Kα radiation, λ = 0.1542 nm). Two-dimensional diffraction patterns were recorded on Fujifilm imaging plates during 1-h exposures and read offline with a Fujifilm BAS 1800-II bioimaging analyzer. Diffraction profiles were calculated by rotationally averaging the 2D patterns.

^{13}C CP/MAS Solid-State Nuclear Magnetic Resonance Spectroscopy. The samples were ground into powder, packed into zirconia rotors, and analyzed using a Bruker Avance III 400 MHz spectrometer (with a ^{13}C frequency of 100.6 MHz). The analysis employed cross-polarization (CP) and magic-angle spinning (MAS) at a spinning speed of 12 kHz, a sweep width of 29,761 Hz, and a recycle delay of 2 s. Each spectrum was averaged over 6,000 scans, and the ^{13}C chemical shifts were calibrated using glycine, with the carboxyl group set at 176.03 ppm.

Thermogravimetric Analysis (TGA). Samples (about 10 mg) were analyzed in a TGA 400 PerkinElmer thermogravimetric analyzer. The heating cycle was performed from 40 to 800 °C at a heating rate of 10 °C min^{-1} under airflow.

Dynamic Mechanical Analysis (DMA). The storage modulus (E'), loss modulus (E''), and tan δ were measured in tension mode using a PYRIS Diamond DMA (PerkinElmer, Waltham, MA, USA). The measurements were performed on thin films (20 mm long, 5 mm wide) at a frequency of 1 Hz, with a heating rate of 2 °C min^{-1} and an amplitude of 10 μm, over a temperature range of −80 to 120 °C.

Moisture Sorption. Film samples (4 cm × 4 cm, 200 μm thick) were dried at 80 °C for 24 h, and then placed in a hermetic container with a controlled degree of humidity kept constant by the presence of saturated salt solutions (NaCl for 75% RH, and $Mg(NO_3)_2$ for 55% RH). The moisture uptake was determined by periodically weighting until a constant mass was reached (m_t). The moisture sorption was calculated using the following equation:

$$\text{moisture sorption} = \frac{m_t - m_0}{m_0} \times 100\% \quad (3)$$

where m_0 is the initial weight of the dry sample and m_t is the weight of the sample at a given time t.

Disintegration of the Films in Vegetable Compost. Samples (4 cm × 4 cm) were buried about 4 cm deep in soil composed of vegetable compost and placed in a closed glass vessel maintained at 58 °C. Water was sprayed once a day to maintain the moisture of the compost. Samples were removed at different times and photographed to visually track the disintegration of the film.

3. RESULTS AND DISCUSSION

Thermoplastization of Bread Waste. BW was successfully extruded by TSE in the presence of glycerol as a plasticizer to produce TPB in the form of a continuous and self-supporting roll that was easily pelletized once cooled to about 50−40 °C. To minimize the risk of degradation during the extrusion process, about 10 wt % water was added to facilitate the plasticization process and reduce the melt viscosity of the plasticized BW. However, even in the presence of water and glycerol, a high level of torque was noted by the TSE, limiting the throughput of the machine and the speed of the screw to less than 50 rpm. Interestingly, all of these issues were completely resolved when MA was added in a proportion between 3 and 5 wt % (based on BW). The extrusion of BW

https://doi.org/10.1021/acssuschemeng.4c06823
ACS Sustainable Chem. Eng. 2024, 12, 15268−15281

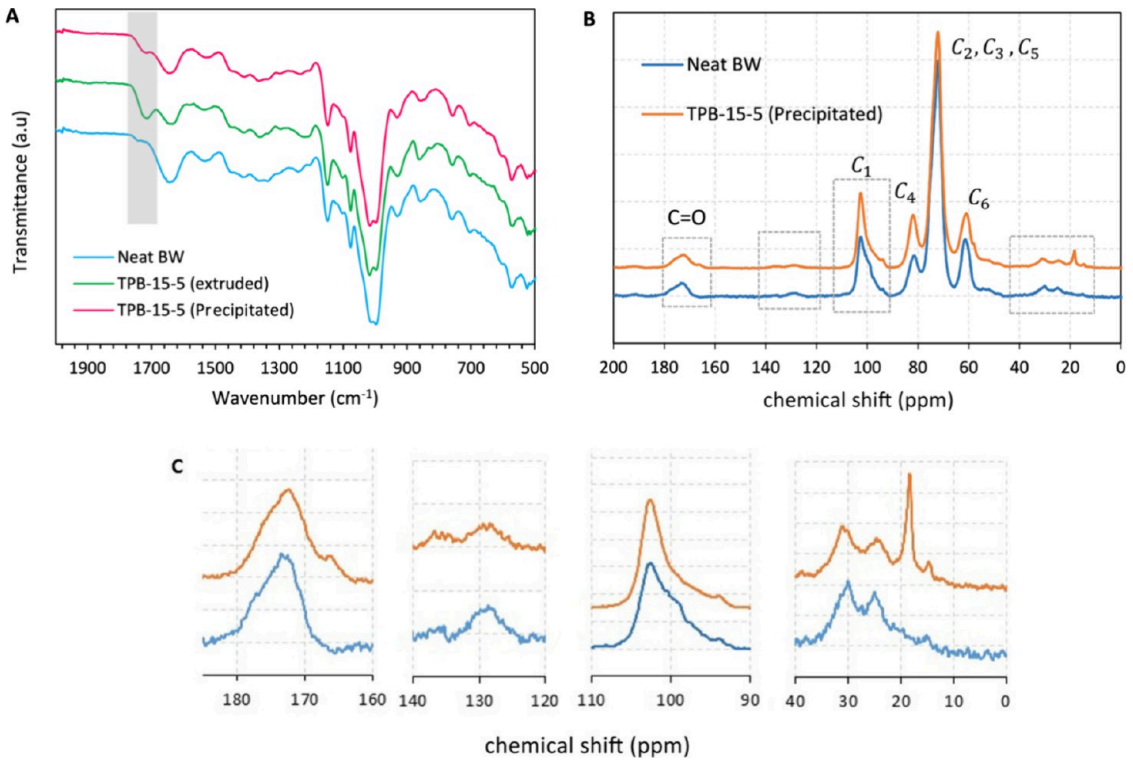

Figure 3. (A) FTIR spectra of neat BW, TPB extruded in the presence of 15 wt % G and 5 wt % M, and precipitated TPB-15-5. (B) ^{13}C solid-state NMR spectra of neat BW and TPB-15-5 and (C) magnification of the 0−40, 90−110, 120−140, and 160−180 ppm regions. TPB was dissolved in DMF and precipitated in methanol to remove free MA.

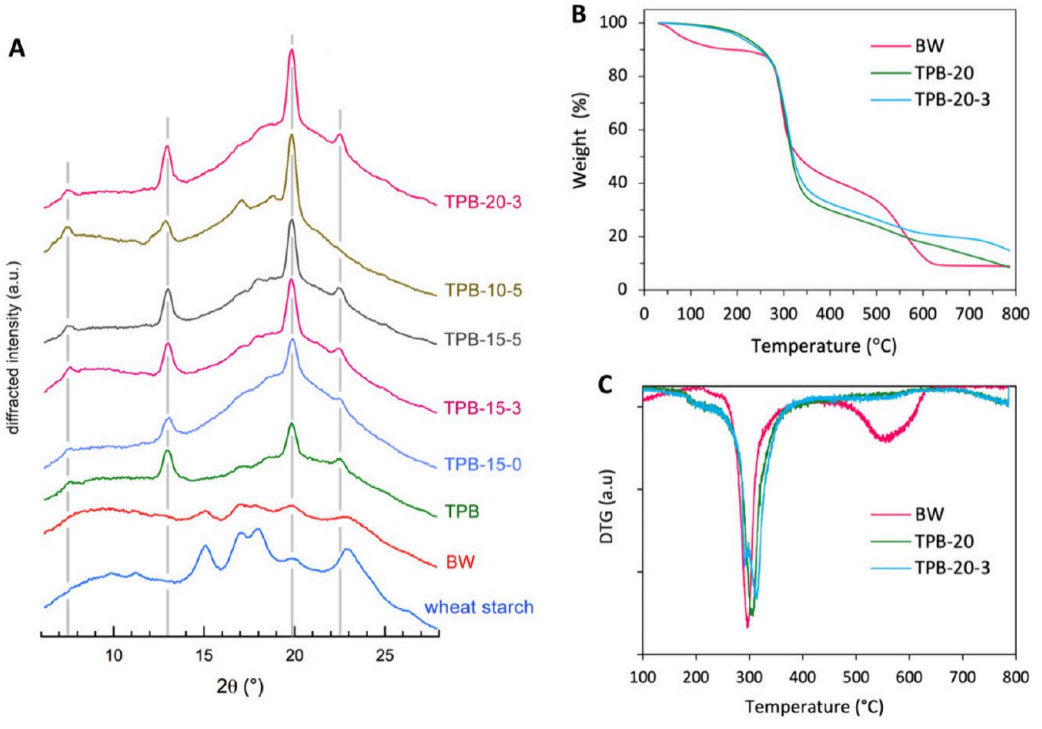

Figure 4. (A) XRD profiles of wheat starch, BW, and TPB plasticized with 10−20 wt % glycerol, and processed without and with MA. The gray vertical lines indicate the peaks from the V-type inclusion complexes. (B) TGA traces of BW and TPB and (C) corresponding DTG plots.

could then be run without an unusual increase in torque, even over a screw speed of 100 rpm. Translucent yellowish TPB pellets were obtained giving rise to an elastic translucid film once pressed at 120 °C, as shown in Figure 2A. The transparency of the TPB film was improved when MA was added as a processing aid.

To gain more insight into the beneficial processing effect of MA, the melt-rheology of the TPB at different amounts of MA and glycerol content (G) was investigated via oscillatory sweep

https://doi.org/10.1021/acssuschemeng.4c06823
ACS Sustainable Chem. Eng. 2024, 12, 15268−15281

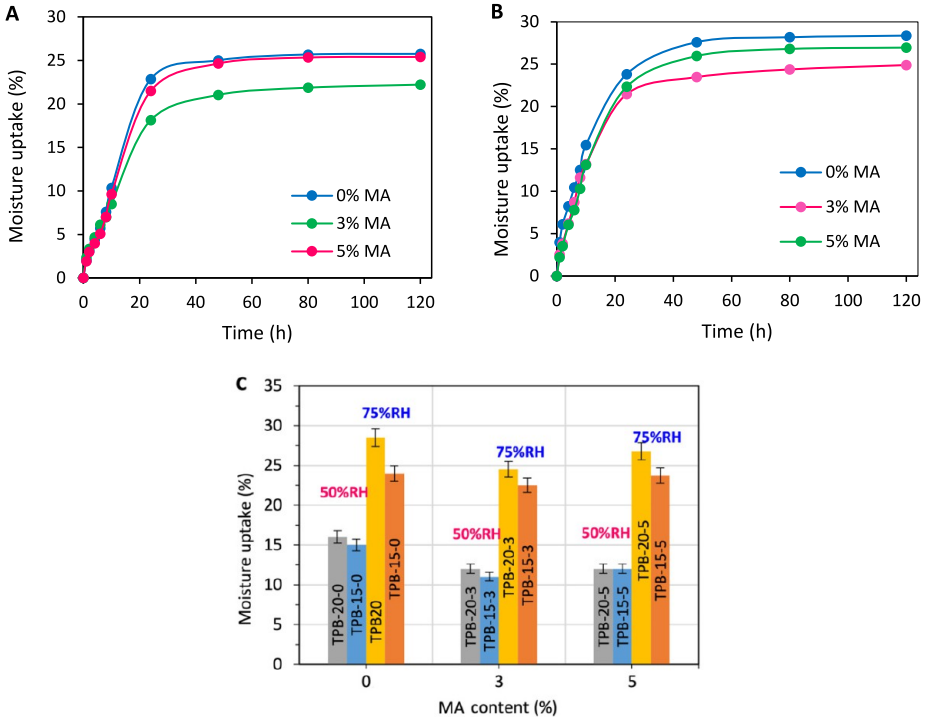

Figure 5. (A, B) Moisture sorption vs time at 75% RH for (A) TPB-15-MA and (B) TPB-20-MA with different MA contents. (C) Equilibrium moisture sorption at 50 and 75% RH for TPB-15-MA and TPB-20-MA with different MA contents.

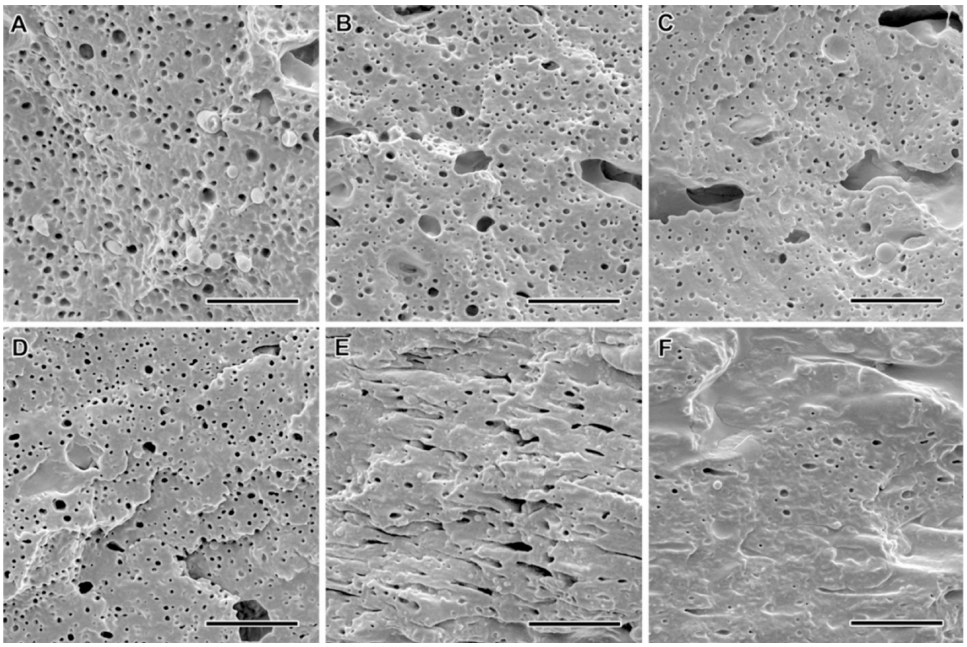

Figure 6. SEM micrographs of the cross-section surface of PBAT/TPB blends with different TPB, glycerol, and PBAT-*g*-MA contents: (A, D) PBAT/TPB 70/30 with 2.5% PBAT-*g*-MA and (A) 20% and (D) 15% glycerol; (B, E) PBAT/TPB 60/40 with 2.5% PBAT-*g*-MA and (B) 20% and (E) 15% glycerol; (C, F) PBAT/TPB 50/50 with 2.5% PBAT-*g*-MA and (C) 20% and (F) 15% glycerol. After cryofracture, the surface of the films was soaked into 1 N HCl to etch away the TPB. Scale bars: 4 μm.

measurements of the storage modulus (G'), loss modulus (G''), and complex viscosity (η^*) as a function of frequency (f). From Figure 2, it can be observed that at 15 and 20 wt % G, and in the absence of MA, TPB exhibited a viscoelastic character with a higher contribution of the elastic effect as G' was higher than G'', especially at 15 wt % G content. The addition of a higher amount of G resulted in a lower elasticity and melt viscosity, which aligns with the plasticizing effect of G. In the presence of MA, the magnitude of G' and G'' decreased by about one decade, and G'' is nearly overlapping with G'. This marked evolution indicates that the melt TPB became less stiff when MA was added during the plasticization process. This evolution was also observed in the η^* which underwent a downward shift, meaning that the resulting

https://doi.org/10.1021/acssuschemeng.4c06823
ACS Sustainable Chem. Eng. 2024, 12, 15268−15281

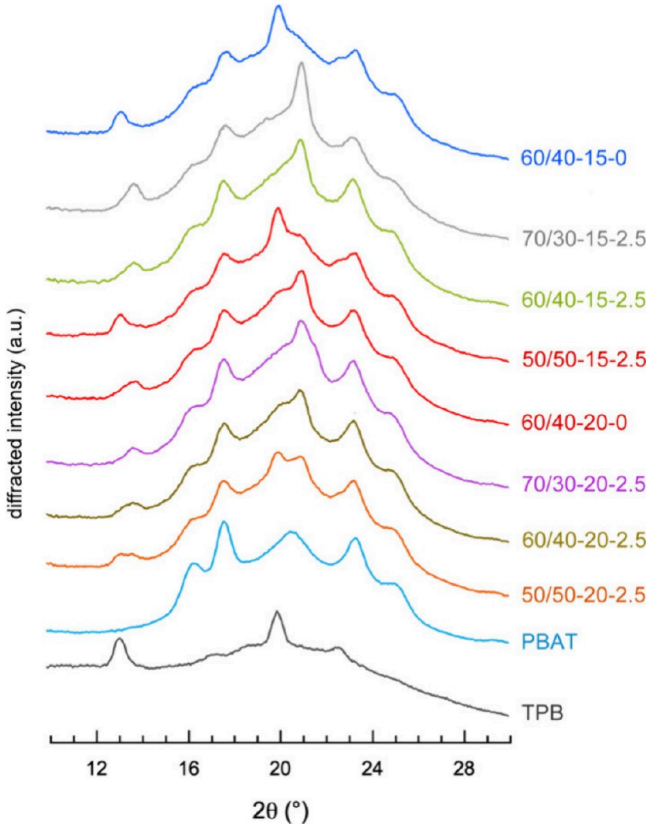

Figure 7. XRD profiles of neat TPB and PBAT and PBAT/TPB-*g*-PBAT-*g*-MA blends.

material became less viscous in the presence of MA. The evolution in G' and η^* explained the easier melt-plasticization of BW when MA was added during the extrusion. When G'' and η^* were high, the polymer was hard to break down and more difficult to flow through the nozzle of the extruder, which explains the increase in the torque observed during the processing of BW in the absence of MA. However, increasing the MA content over 3 wt % did not further alter the magnitude of G', G'', and η^*, as shown in Figure 2B,D where the evolution of G' and η^* versus f at 5 wt % MA was nearly overlapping with that at 3 wt % MA. Two hypotheses may explain the evolution in the viscoelastic properties of melted TPB: (i) the hydrolysis of amylose and amylopectin chains was catalyzed by the acidity of MA in the presence of water molecules; (ii) relatively high temperature facilitated the diffusion of water inside the polymer.

The second hypothesis was the possible esterification of a fraction of hydroxyl groups of BW by MA, thus reducing interaction through hydrogen bonding among amylopectin chains. The FTIR spectra of TPB processed in the presence of 5% MA, and precipitated in methanol to remove the unreacted MA (Figure 3A), showed a weak C═O band at 1720 cm^{-1}, absent in the neat BW, which may originate from the esterification of starch in BW. However, this band was relatively weak, suggesting a low esterification degree of TPB, and thereby ruling out esterification as a significant factor in decreasing the melt-viscosity of TPB when processed in the presence of MA.

The ^{13}C CP/MAS NMR spectra of neat and plasticized BW processed in the presence of MA (TPB-15-5) are shown in Figure 3B. The major signals in the spectrum of BW were associated with the carbons of the starch fraction of the wheat flour, with four typical signals identified: 96−102 ppm for C_1, 70−73 ppm for C_2, C_3, and C_5, 77−83 ppm for C_4, and 59−62 ppm for C_6.[14] Other minor signals from gluten were also seen at 20−35 ppm associated with protein side-chain aliphatic carbons and lipid fraction, and protein main-chain peptide carbonyl carbon (~175 ppm).[15] The weak large signal in the range of 120−130 ppm was likely assigned to protein side-chain aromatic carbons. The main changes in the NMR spectrum of TPB processed in the presence of MA were: (i) the disappearance of the low-intensity peaks at 18 ppm assigned to lipidic material, which may have been lost during the precipitation of MA-treated TPB to remove residual MA; (ii) the signal from the protein fraction in BW did not markedly change after treatment with MA, suggesting no alteration of their chemical structure after extrusion and plasticization process; (iii) a weak peak at 165 ppm emerged in TPB-MA, presumably to the CO signal from grafted MA. The weak intensity of this signal further supports the low extent of esterification of MA on starch contained in BW.

The hypothesis of low esterification extent of MA on BW was also supported by a lack of dependence of the melt-viscoelastic properties on the amount of added MA, as nearly similar viscoelastic behavior was noted at 3 and 5 wt % MA content (Figure 2B,D).

The XRD profiles of wheat starch, BW, and TPB at different glycerol and AM contents are shown in Figure 4A. The profile of wheat starch exhibits an A-type allomorph with peaks at 2θ = 15, 17, 18, 20 and 23.2°.[16] The neat BW was characterized by a broad profile that illustrates the amorphous nature of the material with the presence of A-type peaks of the parent granules that were not completely gelatinized during the bread cooking. In the profile of TPB films, the residual A-type crystallinity disappeared confirming the complete gelatinization of starch during extrusion in the presence of glycerol. The diffraction profile shows that the material was largely amorphous but sharp peaks at 7, 13, 20, and 22.8° were also present. They revealed the presence of a V-type structure likely due to the formation of a fraction of crystalline inclusion complexes between amylose and endogenous lipids present in wheat starch.[17,18]

The onset of thermal degradation of TPB was assessed by TGA. As shown in Figure 4B, the neat BW is characterized by three weight loss events at about 100, 300, and 500 °C, assigned respectively to water evaporation, thermal degradation by depolymerization of polysaccharides and proteins, and carbonization of polymeric material. The derivative curve (DTG) is plotted to help identify the various phenomena relating to the variation in mass (Figure 4C). In BW, the weight loss at 100% is around 10%, due to the presence of adsorbed water. The difference between the degradation profile of BW and TPB is likely due to the presence of glycerol that evaporates around 300 °C, which explains the steeper weight loss for TPB at 300 °C. In TPB, the weight loss started at about 220 °C, presumably due to the evaporation of glycerol, followed by a steep loss at 300 °C corresponding to the thermal degradation of the polysaccharide backbone and gluten protein contained in bread. The residue at 800 °C, approximately 8%, represents the ash content derived from the mineral constituents in the bread. The DTG plots (Figure 4C) for BW display two distinct features: an initial peak at 300 °C attributed to the degradation of polysaccharides and gluten, and a second broader peak at 550 °C, associated with the

https://doi.org/10.1021/acssuschemeng.4c06823
ACS Sustainable Chem. Eng. 2024, 12, 15268−15281

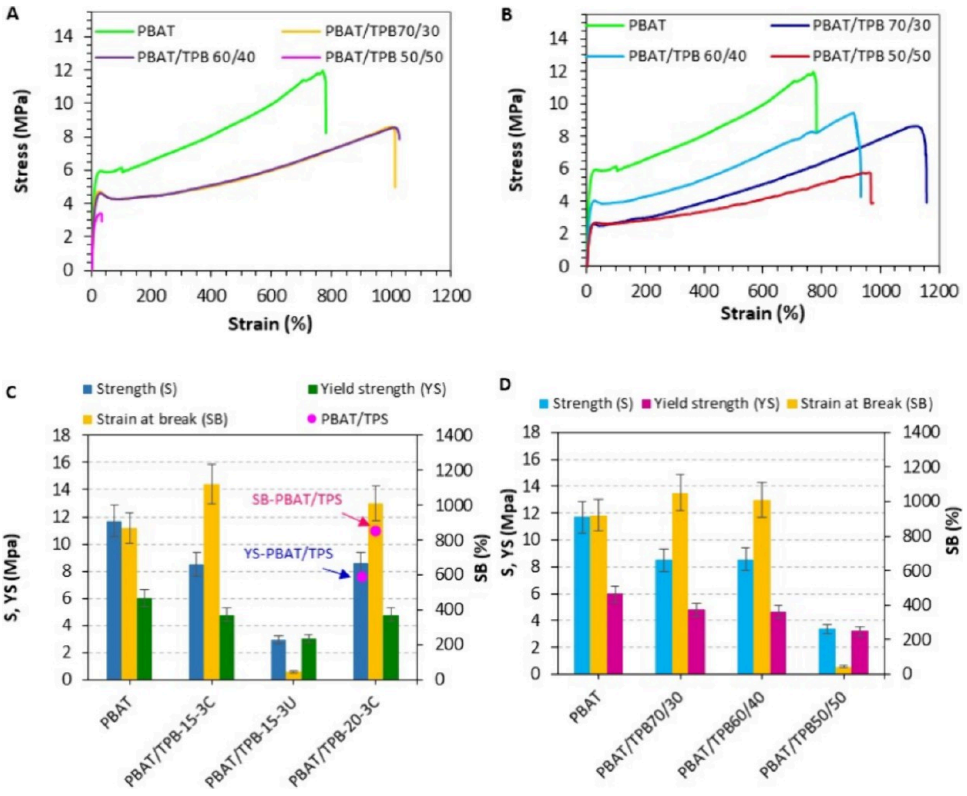

Figure 8. (A, B) Stress−strain plots for PBAT/TPB at different PBAT/TPB ratios for (A) TPB-15-3 and (B) TPB-20-3 in the presence of 2.5 wt % of coupling agent PBAT-*g*-MA. (C, D) Corresponding strength (S), yield strength (YS), and strain at break (SB) for PBAT/TP: (C) PBAT/TPB 70/30 ratio and TPB-15-3 and TPB-20-3 in the presence of the coupling agent PBAT-*g*-MA (labeled C) and without PBAT-*g*-MA (uncoupled, labeled U), and (D) mechanical data for PBAT/TPB blends with different PBAT/TPB ratios (TPB-20-3 and in the presence of the coupling agent). Arrows in (C) point at blends based on PBAT/TPS 60/40 (the data were taken from our previous work[6]),

carbonization of organic material. In TPB, the DTG plot shows a shoulder at 200 °C, resulting from glycerol evaporation, followed by a peak at 300 °C corresponding to the degradation of polysaccharides and gluten.

Given the sensitivity of thermoplasticized starch (TPS) to water and the high fraction of starch in BW, the sorption of water vapor at 50 and 75% RH was investigated. The kinetics of water sorption at 15 and 20 wt % G content and various amounts of added MA are shown in Figure 5. At both RHs, the water absorption was rapid during the first 20 h and gradually leveled off to reach a sorption equilibrium plateau over 40 h. At 55% RH, the plateau sorption rate W_{max} was around 15 wt % for both G contents and slightly decreased to around 12% in the presence of MA (Figure 5C). It increased to around 28 and 24%, at 75% RH, at respective G contents of 15 and 20 wt %, and decreased to about 25 and 23.7% in the presence of MA. The increase in water sorption with increasing RH was due to the higher concentration of water molecules in the atmosphere, driving the water sorption equilibrium to higher values. The increase in G content further increased the hydrophilic character of the TPB, which justifies the increased water sorption, especially at 75% RH. The presence of MA did not significantly affect the water sorption of TPB, presumably due to the inherent hydrophilicity of MA, and its low tendency to react via esterification with the hydroxyl groups of TPB.

Blending TPB and PBAT. For applications in packaging materials, and similarly to starch, TPB needs to be blended with a ductile polyester to mitigate its shortcomings, namely moisture sensitivity, to create a material that can be melt-processed using conventional methods such as injection molding or blown-extrusion. The inclusion of TPB offers several benefits, namely (i) increasing biobased content, (ii) enhancing biodegradability, (iii) improving circularity, and (iv) reducing costs, as polyesters are much more expensive than TPB.

Morphology and Structure of PBAT/TPB Blends. The morphology of the PBAT/TPB blends was analyzed by observing cryofractured films by SEM after the removal of TPB using a chemical etching treatment (Figure 6). As a result, the films became porous and the cavities suggested that TPB existed as dispersed nodules within the PBAT matrix, depending on the PBAT/TPB ratio, the presence or the absence of the coupling agent, and glycerol content in TPB. At 20 wt % G in TPB, and in the presence of a PBAT-*g*-MA coupling agent, the TPB was characterized by a nodular morphology with a size within the 1−2 μm range for the narrower nodules. However, in addition to the population of small nodules, large elongated cavities corresponding to poorly dispersed TPB were seen with a size increasing with the TPB concentration, around 4, 2−5, and 4−8 μm at 30, 40, and 50% TPB, respectively. At 15 wt % G in TPB, the nodular morphology was visible only at the high PBAT/TPB ratio of 70/30. At higher TPB ratios (40 and 50%), the fiber-like morphology was dominant with coexisting nodules (Figure 6E,F).

Referring to literature data, the morphology of immiscible polymer blends is highly complex, influenced by several factors, including the ratio of the blend constituents, their viscoelastic properties, the interfacial tension between them, and the difference in polarity between the phases.[19,20] More specifi-

https://doi.org/10.1021/acssuschemeng.4c06823
ACS Sustainable Chem. Eng. 2024, 12, 15268−15281

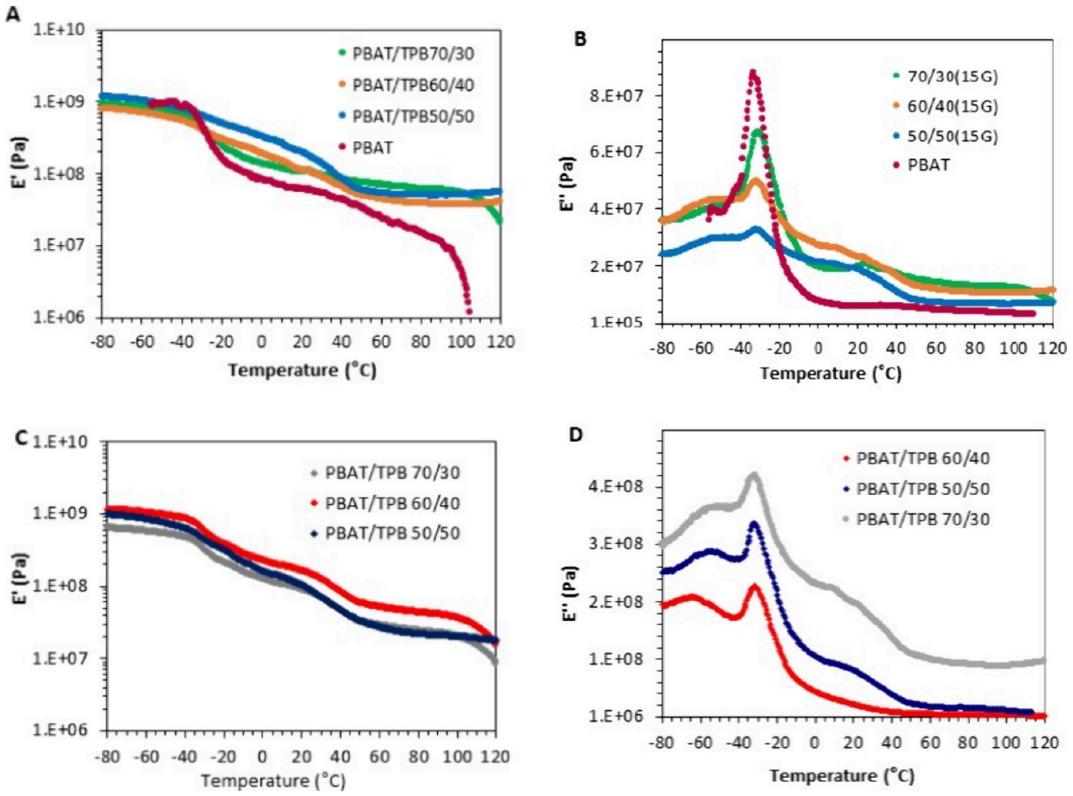

Figure 9. (A, C) Storage tensile modulus E' and (B, D) loss modulus E'' vs temperature at 1 Hz for neat PBAT and PBAT/TPB blends at different ratios and low glycerol content in TPB: (A, B) G = 15 wt %; (C, D) G = 20 wt %. All blends were processed in the presence of 2.5 wt % PBAT-*g*-MA.

cally, the melt viscosity of the blend components and their viscoelastic properties play a significant role in controlling the morphology development of polymer blends, and the domain size of the minor component. Higher-viscosity polymers tend to phase-separate more slowly than low-viscosity polymers because they resist molecular diffusion and flow. This explains the fibrillar morphology observed in blends with TPB plasticized with 15 wt % G. The high viscosity and elastic character of TPS at 15 wt % G contribute to stabilizing the elongated structure formed by the deformation of the TPS phase parallel to the flow direction. On the other hand, at 20 wt % G, the lower viscosity facilitated the deformation and breakdown of TPB during processing allowing the deformed structure to relax more readily into spheroidal shapes.

The XRD profiles of PBAT/TPB blends are shown in Figure 7. The profile of neat PBAT contains five main peaks at 2θ = 16.3, 17.6, 20.5, 23.3, and 24.9°, consistent with our previous data.[21] The profiles of the blends exhibited peaks from both PBAT and TPB constituents with relative intensities that depended on the PBAT/TPB proportion. The contribution of TPB was identified by peaks corresponding to the V-type amylose-lipid crystalline complexes. The persistence of PBAT diffraction peaks in PBAT/TPB blends indicated that the inclusion of TPB did not hamper the crystallization aptitude of PBAT, which is of great benefit for the mechanical performance of the film, as the PBAT crystalline phase would enhance the stiffness and the strength of the film.

Mechanical Properties of PBAT/TPB Blends. The mechanical properties of PBAT/TPB blends were investigated by tensile tests and DMA measurements on film with varying TPB content. The typical stress−strain plots of PBAT/TPB blends are presented in Figure 8A,B, from which the strength (S), yield-strength (YS), and strain at break (SB) were extracted and are shown in Figure 8C,D. For the different coupled blends, three regions were distinguished, the first one in the low strain deformation (<10%) corresponded to the elastic character, the second up to approximately 200% corresponded to the plastic deformation of the film after yielding and formation of a neck, and the third region over 300% strain correspond to the strain hardening of the material with an increase in the stress until the film breaks. The inclusion of TPB in the PBAT matrix was accompanied by a reduction in YS and SB, with the magnitude of this reduction being attenuated when PBAT-*g*-MA was used as a compatibilizer. For instance, in blends containing 40 wt % TPB plasticized with 15 wt % G (60/40−15), the S and SB achieved 8.55 MPa and 1000% for the coupled samples, compared to 2.9 MPa and 36% for the uncoupled blend. This effect was also observed in PBAT/TPS blends and is explained by the fact that the TPB phase as well as TPS have a low strength and are dispersed in the PBAT matrix in the form of nodules as long as their content is lower than 50 wt %.

Without a compatibilizer, the dispersed nodules acted as stress concentrators and resulted in the premature breaking of the material. When the blend was processed in the presence of PBAT-*g*-MA coupling agent, the interfacial adhesion between the TPB and PBAT phases was enhanced, promoting more efficient stress transfer between the PBAT matrix to the dispersed phase. This justified the marked improvement in the ductility and strength of the blend. The efficiency of PBAT-*g*-MA compatibilizers is well documented in the literature and is explained by the formation of ester linkages between the MA

https://doi.org/10.1021/acssuschemeng.4c06823
ACS Sustainable Chem. Eng. 2024, 12, 15268−15281

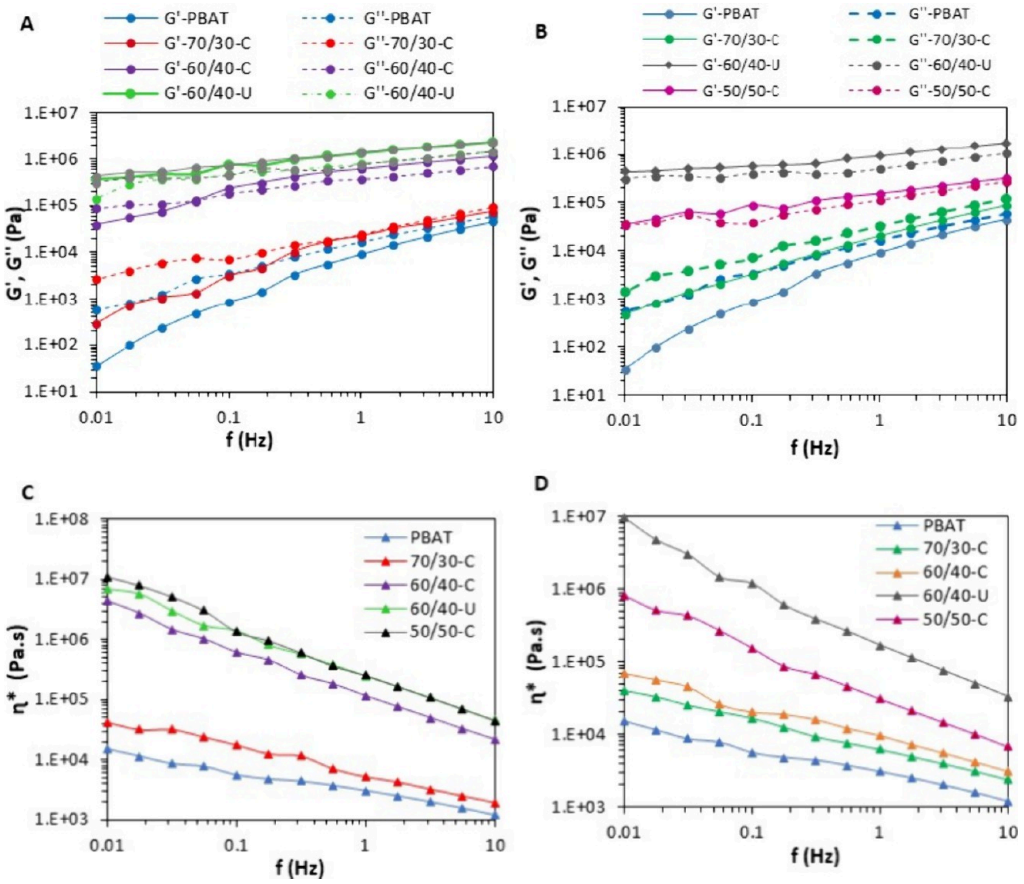

Figure 10. (A, B) Storage modulus (G') and loss modulus (G'') vs frequency (f) at 150 °C for PBAT/TPB blends at different ratios PBAT/TPB: (A) TPB-15-3 and (B) TPB-20-3. (C, D) Corresponding complex viscosity (η^*) for (C) TPB-15-3 and (D) TPB-20-3. C and U refer to coupled and uncoupled blends.

grafted onto PBAT and TPS.[22] Interestingly, it can be seen that the PBAT/TPB blends with TPB plasticized with 20% G, maintained a high ductility even with 50 wt % TPB, achieving an S and SB of around 6 MPa and 900%, respectively, respectively. For comparison, YS and SB for blends prepared with PBAT and TPS at similar G content were included in Figure 8C. When starch was used instead of BW, a better YS at around 7−8 MPa was achieved, while the SB reached a high level (>700−800%) like for TPB.

The DMA analysis provided further insight into the changes in material stiffness with temperature and the different relaxations of the polymer phases by examining the evolution of the storage modulus (E') and loss modulus (E''), respectively (Figure 9). Neat PBAT is characterized by a glass transition temperature (T_g) around −27 °C, marked by a maximum in E" trace, and a drop in E' of about 2 orders of magnitude, followed by a sharp decline in E' above 100 °C due to the melting of the crystalline phase from PBAT. In PBAT/TPB blends, the thermogram is typical of immiscible polymer blends, incorporating the contribution of both PBAT and TPB phases as shown in Figure 9A. The material remains rigid up to −30 °C, with E' around 1 GPa, and then E' starts decreasing progressively beyond the T_g of the PBAT phase. However, the magnitude of E' decay became less pronounced as the content in PBAT decreased. In addition, unlike neat PBAT, which becomes sticky above 100 °C, the PBAT/TPB blend retained its elastic character over 100 °C, as evidenced by the level of E' staying within the 300−500 MPa range. In E'' traces, three relaxations were observed (Figure 9B), the first around −50 °C, attributed to the relaxation of the starch phase rich in glycerol in TPB; the second, corresponding to the T_g of PBAT around −30 °C; and the third, a broad hump between 0 and 45 °C, attributed to the glass transition temperature of the starch-rich phase.[23]

The increase in the fraction of PBAT in the PBAT/TPB blends resulted in a more pronounced relaxation of the PBAT phase at the expense of the TPB one. The increase in the glycerol content (G) in the TPB phase (TPB-20) of the blend (Figure 9C and 9D), resulted in a shift to a lower temperature of the glass transition of the TPB phase, without affecting that of the PBAT matrix. This was expected as more glycerol increased the ductility of the TPB phase.

Melt Rheology of the PBAT/TPB Blends. The melt rheology of the PBAT/TPB blends with varying TPB content was studied at 150 °C by measuring the storage modulus (G'), loss modulus (G''), and complex viscosity (η^*) as a function of frequency (f) in the linear viscoelastic region (Figure 10). The neat PBAT matrix exhibited a liquid-like character, G'' being significantly higher than G' (more than 1 order of magnitude over the entire frequency domain) (Figure 10C,D). The complex viscosity, η^*, of PBAT displayed a shear-thinning behavior over throughout the entire frequency range, consistent with previous findings (Figure 10C,D).[13]

In the PBAT/TPB blends, the addition of TPB resulted in an upward shift in both the G' and G'' traces compared to the neat PBAT matrix. The storage modulus G' became almost

https://doi.org/10.1021/acssuschemeng.4c06823
ACS Sustainable Chem. Eng. 2024, 12, 15268−15281

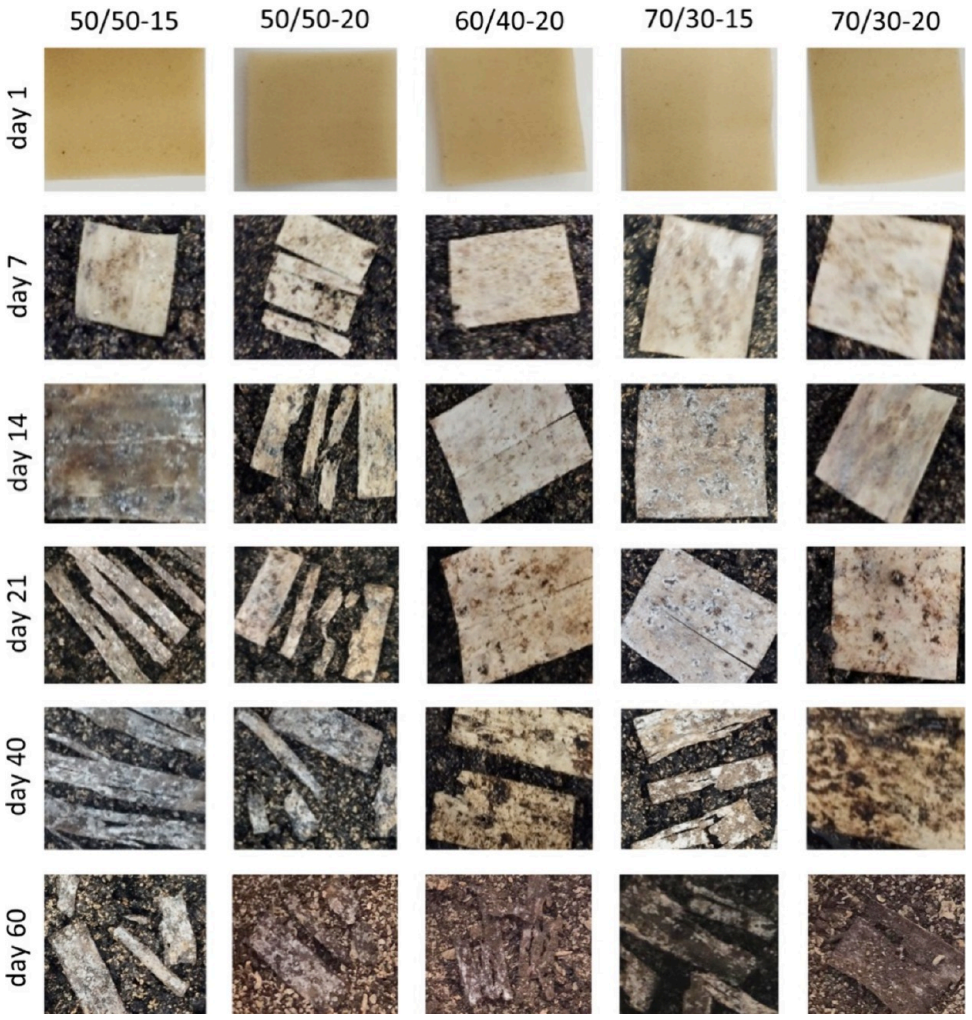

Figure 11. Evolution of the PBAT/TPB-G films with burial time in the soil at 58 °C.

indistinguishable from G'' and showed less dependence on frequency. This suggests that incorporating TPB enhanced the elastic properties of the melt PBAT/TPB blend, with stiffness increasing as the TPB content rose. This effect was further supported by the complex viscosity η^*, which also increased with higher TPB content, indicating greater melt viscosity. The impact was more significant when TPB had lower plasticizer content and when the blend was processed without a coupling agent. This evolution was expected in polymer blends, with a general trend being that the G' and viscosity values of blends have intermediate values between those of both polymers weighed by their volume fraction,[24] especially when a good interfacial adhesion is achieved. This justifies that in PBAT/TPB blends with the same content in TPB, but with a higher amount of plasticizer in TPB, lower levels in G' and η^* were reached. The higher G content in TPB made TPB less stiff and viscous at melt, as previously noted. It is worth mentioning that a similar trend in the evolution of the melt-rheological properties was observed in blends based on TPS and biodegradable polyesters such as PCL,[25] PLA,[26] and PBAT,[13] especially when the blend was processed in the presence of a compatibilizing agent to improve the interfacial adhesion between the hydrophobic polyester matrix and hydrophilic TPS phase.

Disintegration under Burial Conditions. A qualitative evaluation of the biodegradation of PBAT/TPB blends was conducted by inspecting the disintegration of the film buried in the soil and maintained at 58 °C. Figure 11 illustrates the evolution of the films after different burial times. It shows that the film started fragmenting over a two-week burial time and the disintegration progressed. However, the extent of fragmentation seemed to be favored with increasing TPB content. The breakdown of the PBAT/TPB film resulted from the chemical decomposition induced by microorganisms in the compost. The easier degradation of TPB, favored by its polysaccharidic nature, explains the higher propensity of disintegration of PBAT/TPB to disintegrate at higher TPB contents.

Although more accurate standard tests for biodegradation should be performed by monitoring the CO_2 release over time at 58 °C and under aerobic conditions, it provides an easy assessment of the susceptibility of plastics to biodegradation, as the disintegration into fragments during the first phase of degradation.[27]

Pilot-Scale Production of Thin Films by Blown Extrusion. Since the primary application of biodegradable plastics based on starch blends focuses on thin films produced by blown extrusion, a pilot test was conducted using a PBAT/TPB blend to explore the potential for starch substitution by BW.TPB processed with 20 wt % G and 3 wt % MA was selected for this test as well as the PBAT/TPB 60/40 blend that included 2 wt % PBAT-*g*-MA as a coupling agent to

https://doi.org/10.1021/acssuschemeng.4c06823
ACS Sustainable Chem. Eng. 2024, 12, 15268−15281

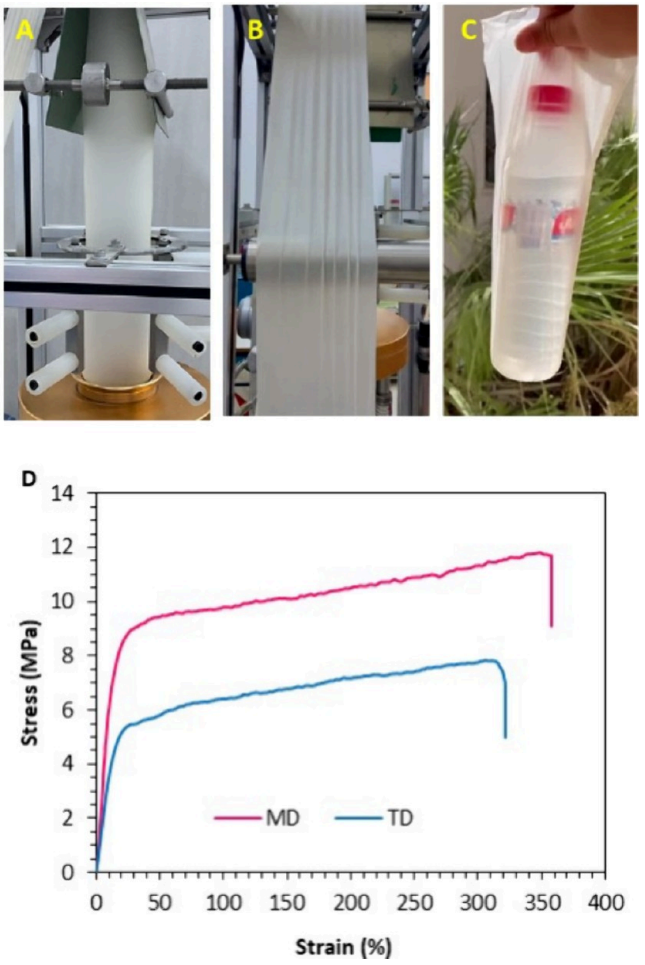

Figure 12. (A, B) Photographs showing the aspect of the PBAT/TPB 60/40-20-3 bubble film during the blowing process. (C) Bags prepared from the processed film. (D) Stress−strain plots of the thin film prepared by blown extrusion recorded along the machine direction (MD) and transverse direction (TD).

improve the interfacial adhesion between PBAT and TPB. TPB pellets were first prepared by twin-screw extrusion (TSE) at 130 °C with the addition of 10 wt % water to facilitate the extrusion. The PBAT, TPB, and PBAT-*g*-MA mixture was melt-mixed by TSE, and pelletized into monodisperse granules ready for use. The pellets were fed to the hopper of a single-screw film-blowing pilot extruder (screw diameter 20 mm, L/D: 28:1), and the blown extrusion process was performed according to an optimized temperature profile. Film blowing was conducted with BUR-DDR values of 1.6 and 12.5 respectively, resulting in a stable and continuous bubble without melt fracture, fluttering, or bubble breathing of the blown film (Figure 12A,B).

The tensile properties of the films were tested along the machine direction (MD) and the transverse direction (TD), with the stress−strain trace shown in Figure 12D. Better mechanical properties of the blown film were achieved along MD in comparison with TD in terms of strength, ultimate strength, and tensile modulus. This effect was likely due to the anisotropy of the film induced by the orientation of the PBAT chains imposed by stresses during fabrication. Three main factors contribute to this orientation: (i) flow of the melt through the die where the resulting orientation is along MD, (ii) stress induced by the drawing of the melt via the nip rolls, causing orientation along MD, and (iii) orientation along TD resulting from the blowing process. Similar results were observed in our previous work.[28] It is also worth noting that the blown film exhibited better S and YS along both directions compared to the film produced by flat-die extrusion at the same PBAT/TPB ratio and G content, although a lower SB was observed for the former. This effect may be attributed to the orientation of PBAT chains during the blowing process.

One may consider the viability of the potential industrial use of BW in bioplastic processing, considering the need for a consistent supply of BW in sufficient amounts and with reliable quality. The strategies used for other recyclable materials like plastics, metals, or glass could be adapted for BW through the following approaches: (i) Enhancing waste collection by providing dedicated bins or containers for bread waste in bakeries, supermarkets, and other facilities; (ii) Establishing partnerships with waste management companies that specialize in organic or food waste to ensure proper handling and processing of bread waste; (iii) Raising awareness among stakeholders, such as bakeries, supermarkets, and restaurants, about the importance of collecting bread waste. It is worth noting that in many countries, these approaches are already in practice, with companies specializing in the collection of BW. For example, in Tunisia and Morocco, BW is used as an additive in poultry feed, partially replacing the more expensive wheat.

4. CONCLUSION

BW was successfully thermoplasticized by melt-processing and blended with PBAT to replace food-grade starches in the production of biodegradable plastics based on blends of polyester and thermoplasticized starch (TPS). BW was extruded by TSE in the presence of glycerol as a plasticizer to produce TPB. However, the addition of a small amount (2.5 wt %) of MA was necessary to facilitate the extrusion and prevent the degradation of TPB. The hypothesis of the hydrolysis reaction of amylose and amylopectin chains catalyzed by the acidity of MA was suggested to explain the improved processing of TPB by the addition of MA. This hypothesis was supported by rheological measurements which showed a significant decrease in G' and G'' by about an order of magnitude for TPB processed in the presence of MA, compared to the TPB processed without MA, and containing the same amount of glycerol. XRD data indicated that TPB had a predominantly amorphous character with a fraction of V-type single-helical inclusion compounds likely resulting from the recrystallization of amylose with endogenous lipids. The TGA data revealed the good thermal stability of TPB up to 200 °C presumably due to the evaporation of glycerol, followed by a steep loss at 250 °C corresponding to the thermal degradation of starch. The blending of TPB with PBAT at a fraction between 30 and 50 wt % using TSE yielded a composite material where TPB was dispersed as nodules. In the presence of PBAT-*g*-MA as a coupling agent, the PBAT/TPB blends achieved mechanical performance close to that of neat PBAT, with a strength in the range of 8−9 MPa, and a strain at break exceeding 900%, for composites containing up to 40 wt % TPB. A pilot-scale blown extrusion test was conducted for a PBAT/TPB blend at a 60/40 ratio giving a uniform 30 μm-thick film without defects. This proof of concept demonstrated the potential for replacing of food-grade starch with BW in PBAT, with potential applications in biodegradable plastics including consumer bags, packaging

https://doi.org/10.1021/acssuschemeng.4c06823
ACS Sustainable Chem. Eng. 2024, 12, 15268−15281

film, agricultural mulch film, and silage wraps. BW offers a more sustainable alternative to commercial starches that do not compete with food chains. In addition, given the availability of cheap BW, we expect an economic benefit from replacing edible starch by BW.

The present work is the first report on the replacement of starch with BW in biodegradable plastics based on starch blends. Considering the availability and cheapness of BW, and the competitiveness of the mechanical performance of films derived from PBAT/TPB blends, with those derived from their counterparts using starch, this approach would contribute to a more sustainable route for the production of biodegradable plastics as part of a circular economy.

AUTHOR INFORMATION

Corresponding Author

Sami Boufi − *LMSE, Faculty of Science, University of Sfax, 3018 Sfax, Tunisia;* orcid.org/0000-0002-3153-0288; Phone: 216 47274400; Email: sami.boufi@fss.rnu.tn; Fax: 216 74274437

Authors

Samar Bouzidi − *LMSE, Faculty of Science, University of Sfax, 3018 Sfax, Tunisia*

Jean-Marc Lévèque − *Univ. Grenoble Alpes, CNRS, Grenoble INP, LRP, F-38000 Grenoble, France;* orcid.org/0000-0003-3033-7141

Albert Magnin − *Univ. Grenoble Alpes, CNRS, Grenoble INP, LRP, F-38000 Grenoble, France*

Sonia Molina-Boisseau − *Univ. Grenoble Alpes, CNRS, CERMAV, F-38000 Grenoble, France*

Jean-Luc Putaux − *Univ. Grenoble Alpes, CNRS, CERMAV, F-38000 Grenoble, France;* orcid.org/0000-0002-9760-5369

Complete contact information is available at: https://pubs.acs.org/10.1021/acssuschemeng.4c06823

Notes

The authors declare no competing financial interest.

ACKNOWLEDGMENTS

The authors gratefully acknowledge LabEx Tec 21 (Investissements d'Avenir #ANR-11-LABX-0030), Partenariat Hubert Curien Utique (CMCU Project 23G1118), and the Glyco@Alps Programme (Investissements d'Avenir #ANR-15-IDEX-02) for financial support. We thank the NanoBio-ICMG Platform (UAR 2607, Grenoble) for granting access to the Electron Microscopy and NMR facilities as well as Christine Lancelon-Pin and Patricia Chaud (CERMAV) for the SEM observations and NMR analysis, respectively. CERMAV and LRP are part of Institut Carnot PolyNat (Investissements d'Avenir #ANR-11-CARN-030-01). We also thank the Ministry of Higher Education and Research of Tunisia for financial support (Project 21P2ES-D6P3).

REFERENCES

(1) Geyer, R.; Jambeck, J. R.; Law, K. L. Production, Use, and Fate of All Plastics Ever Made. *Sci. Adv.* **2017**, *3* (7), e1700782.

(2) *Plastics − The Facts 2018: An Analysis of European Plastics Production, Demand and Waste Data*. PlasticsEurope, 2018. https://plasticseurope.org/wp-content/uploads/2021/10/2018-Plastics-the-facts.pdf.

(3) Eerkes-Medrano, D.; Thompson, R. C.; Aldridge, D. C. Microplastics in Freshwater Systems: A Review of the Emerging Threats, Identification of Knowledge Gaps and Prioritisation of Research Needs. *Water Res.* **2015**, *75*, 63−82.

(4) *Bioplastics Market Development Update 2023*. European Bioplastics, December 2023. https://docs.european-bioplastics.org/publications/market_data/2023/EUBP_Market_Data_Report_2023.pdf.

(5) Surendren, A.; Mohanty, A. K.; Liu, Q.; Misra, M. A Review of Biodegradable Thermoplastic Starches, Their Blends and Composites: Recent Developments and Opportunities for Single-Use Plastic Packaging Alternatives. *Green Chem.* **2022**, *24* (22), 8606−8636.

(6) Dammak, M.; Fourati, Y.; Tarrés, Q.; Delgado-Aguilar, M.; Mutjé, P.; Boufi, S. Blends of PBAT with Plasticized Starch for Packaging Applications: Mechanical Properties, Rheological Behaviour and Biodegradability. *Ind. Crops Prod.* **2020**, *144*, 112061.

(7) Kasirajan, S.; Ngouajio, M. Polyethylene and Biodegradable Mulches for Agricultural Applications: A Review. *Agron. Sustainable Dev.* **2012**, *32* (2), 501−529.

(8) Akhir, M. A. M.; Mustapha, M. Formulation of Biodegradable Plastic Mulch Film for Agriculture Crop Protection: A Review. *Polym. Rev.* **2022**, *62* (4), 890−918.

(9) Sükrü Demirci, A.; Palabıyık, I.; Gümüs, T.; Özalp, Ş. Waste Bread as a Biomass Source: Optimization of Enzymatic Hydrolysis and Relation between Rheological Behavior and Glucose Yield. *Waste Biomass Valorization* **2017**, *8* (3), 775−782.

(10) Mihajlovski, K.; Rajilić-Stojanović, M.; Dimitrijević-Branković, S. Enzymatic Hydrolysis of Waste Bread by Newly Isolated Hymenobacter Sp. CKS3: Statistical Optimization and Bioethanol Production. *Renewable Energy* **2020**, *152*, 627−633.

(11) Leung, C. C. J.; Cheung, A. S. Y.; Zhang, A. Y.-Z.; Lam, K. F.; Lin, C. S. K. Utilisation of Waste Bread for Fermentative Succinic Acid Production. *Biochem. Eng. J.* **2012**, *65*, 10−15.

(12) Mevliyaoğulları, E.; Karslı, M. A.; Mert, B. Utilizing Surplus Bread as an Ingredient in Dog Food: Evaluating Baking and Extrusion Processing on Physicochemical Properties and in Vitro Digestibility Performance. *J. Cereal Sci.* **2023**, *113*, 103741.

(13) Fourati, Y.; Tarrés, Q.; Mutjé, P.; Boufi, S. PBAT/Thermoplastic Starch Blends: Effect of Compatibilizers on the Rheological, Mechanical and Morphological Properties. *Carbohydr. Polym.* **2018**, *199*, 51−57.

(14) Singh, V.; Ali, S. Z.; Divakar, S. ^{13} C CP/MAS NMR Spectroscopy of Native and Acid Modified Starches. *Starch - Stärke* **1993**, *45* (2), 59−62.

(15) Garbow, J. R.; Schaefer, J. Magic-Angle Carbon-13 NMR Study of Wheat Flours and Doughs. *J. Agric. Food Chem.* **1991**, *39* (5), 877−880.

(16) Lourdin, D.; Putaux, J.-L.; Potocki-Véronèse, G.; Chevigny, C.; Rolland-Sabaté, A.; Buléon, A. Crystalline Structure in Starch. In *Starch*; Springer: Tokyo, 2015; pp 61−90. DOI: 10.1007/978-4-431-55495-0_3.

(17) van Soest, J. J. G.; Hulleman, S. H. D.; de Wit, D.; Vliegenthart, J. F. G. Crystallinity in Starch Bioplastics. *Ind. Crops Prod* **1996**, *5* (1), 11−22.

(18) Le, C.-A.-K.; Choisnard, L.; Wouessidjewe, D.; Putaux, J.-L. Polymorphism of Crystalline Complexes of V-Amylose with Fatty Acids. *Int. J. Biol. Macromol.* **2018**, *119*, 555−564.

(19) Pötschke, P.; Paul, D. R. Formation of Co-Continuous Structures in Melt-Mixed Immiscible Polymer Blends. *J. Macromol. Sci. C: Polym. Rev.* **2003**, *43* (1), 87−141.

(20) Li, G.; Favis, B. D. Morphology Development and Interfacial Interactions in Polycaprolactone/Thermoplastic-Starch Blends. *Macromol. Chem. Phys.* **2010**, *211* (3), 321−333.

(21) Aouay, M.; Magnin, A.; Lancelon-Pin, C.; Putaux, J.-L.; Boufi, S. Mitigating the Water Sensitivity of PBAT/TPS Blends through the Incorporation of Lignin-Containing Cellulose Nanofibrils for Application in Biodegradable Films. *ACS Sustainable Chem. Eng.* **2024**, *12* (29), 10805−10819.

(22) Nabar, Y.; Raquez, J. M.; Dubois, P.; Narayan, R. Production of Starch Foams by Twin-Screw Extrusion: Effect of Maleated Poly(Butylene Adipate- *Co* -Terephthalate) as a Compatibilizer. *Biomacromolecules* **2005**, *6* (2), 807−817.
(23) Forssell, P. M.; Mikkilä, J. M.; Moates, G. K.; Parker, R. Phase and Glass Transition Behaviour of Concentrated Barley Starch-Glycerol-Water Mixtures, a Model for Thermoplastic Starch. *Carbohydr. Polym.* **1997**, *34* (4), 275−282.
(24) Robeson, L. M. Fundamentals of Polymer Blends. In *Polymer Blends: A Comprehensive Review*; Hanser, 2007; Chapter 2, pp 11−23.
(25) Shin, B.; Lee, S.; Shin, Y.; Balakrishnan, S.; Narayan, R. Rheological, Mechanical and Biodegradation Studies on Blends of Thermoplastic Starch and Polycaprolactone. *Polym. Eng. Sci.* **2004**, *44* (8), 1429−1438.
(26) Shin, B. Y.; Jo, G. S.; Kang, K. S.; Lee, T. J.; Kim, B. S.; Lee, S. Il; Song, J. S. Morphology and Rheology on the Blends of PLA/CMPS. *Macromol. Res.* **2007**, *15* (4), 291−301.
(27) Sintim, H. Y.; Bary, A. I.; Hayes, D. G.; Wadsworth, L. C.; Anunciado, M. B.; English, M. E.; Bandopadhyay, S.; Schaeffer, S. M.; DeBruyn, J. M.; Miles, C. A.; Reganold, J. P.; Flury, M. In Situ Degradation of Biodegradable Plastic Mulch Films in Compost and Agricultural Soils. *Sci. Total Environ.* **2020**, *727*, 138668.
(28) Bouzidi, S.; Ben Ayed, E.; Tarrés, Q.; Delgado-Aguilar, M.; Boufi, S. Processing Polymer Blends of Mater-Bi® and Poly-L-(Lactic Acid) for Blown Film Application with Enhanced Mechanical Strength. *Polymers (Basel)* **2023**, *15* (1), 153.

https://doi.org/10.1021/acssuschemeng.4c06823
ACS Sustainable Chem. Eng. 2024, 12, 15268−15281